Received: 14 January 2021 | Revised: 29 March 2021 | Accepted: 12 April 2021

DOI: 10.1002/ctpp.202100017

ORIGINAL ARTICLE

Contributions to Plasma Physics

Numerical investigation of the plasma processes for propellant heating in electrothermal plasma thruster for nanosatellites

Stoil Ivanov | **Stanimir Kolev** | **Zhivko Kiss'ovski**

Radiophysics and Electronics Department, Faculty of Physics, Sofia University "St. Kl. Ohridski", Sofia, Bulgaria

Correspondence
Stoil Ivanov, Faculty of Physics, Sofia University "St. Kl. Ohridski", 5 James Bourchier Blvd, 1164 Sofia, Bulgaria.
Email: stoil.ivanov@phys.uni-sofia.bg

Funding information
Bulgarian Ministry of Education Science Fund, Grant/Award Number: KP-06-OPR 01/1; National Research Programme "Young scientists and postdoctoral students", Grant/Award Number: 577/17.08.2018; Ministry of Education

Abstract

Numerical investigation of the plasma processes in a cylindrical chamber with small dimensions of a novel microwave electrothermal plasma thruster for nanosatellites has been conducted. The absorbed microwave power from the electrons in the plasma column of the surface wave discharge is included in the computational model as a heat source with Gaussian distribution. The computational model takes into account the elastic and inelastic collisions of the electrons with the atoms in the ground state and two excited states (−s, −p) and the processes of recombination and deactivation of the plasma species in the volume and on the walls of the chamber. The computational model includes the flow of neutral gas and the processes in the plasma for effective heating of neutral particles by collisions not only with electrons but also with ions. Selected combinations of input power and propellant mass flow rates are used as initial parameters for the numerical investigation. The results show that at higher mass flow rates the heating of the neutral gas is more effective and at power levels of 4 W and propellant mass flow rate of 3 mg/s the electrothermal plasma thruster demonstrates effective performance and thrust levels in the order of 1 mN.

KEYWORDS

electrothermal thruster, nanosatellite, plasma, propulsion

1 | INTRODUCTION

The nanosatellites are becoming more and more popular satellite platforms due to the substantial advancement of electronics in the past couple of decades. The electrical components have decreased their size and mass, which enable smaller satellites to carry out tasks that traditionally have been undertaken by larger and heavier satellite platforms. Subsequently, the nano/microsatellite market forecast[1] is showing increase in launches during 2021 and the following years. However, there is still a growing need for propulsion systems, which could fit the size, mass and power limitations coming with the nanosatellites (mass up to 10 kg). The applications vary from constellation orbit maintenance[2,3] to space debris mitigation in low Earth orbit, which is another pressing issue threatening the modern space exploration.[4] The long-standing propulsion technologies are experiencing difficulties when miniaturization is at hand and their efficiency decreases with decreasing size and power consumption.[5] This is why new concepts of small thrusters are developed.[6–8] The electrothermal plasma thrusters have many advantages such as small dimensions, light weight and low power consumption.[9] For the simultaneous modelling of the energy supply system, the plasma processes in the plasma source and the gas flow, it is appropriate to use the COMSOL software package.[10–12]

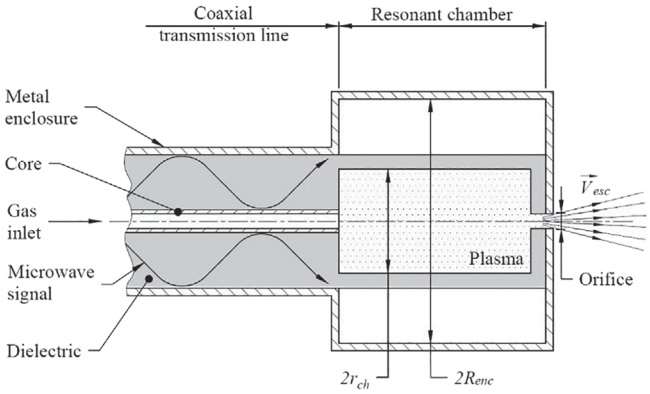

FIGURE 1 Schematic of electrothermal microwave plasma thruster

The electric propulsion technologies for satellites are gaining popularity and are becoming the preferred choice over chemical thrusters. The main reason is that the chemical thrusters use the energy stored in the propellant, which is limited to the energy of the molecular bonds in it, while the electrothermal thrusters use the available onboard electrical energy to accelerate the propellant. The electrical energy is normally stored in batteries and generated by an onboard power generator (e.g., photovoltaic module, radioisotope thermoelectric generator). This allows the electrical propulsion thrusters to characterize with larger specific impulse, which is to use the onboard propellant more efficiently.

The electrical propulsion technologies are roughly divided into three types: electrothermal, electromagnetic and electrostatic. Numerous R&D projects using all three approaches exist but here the electrothermal type is emphasized because of the possibility to utilize surface wave discharge and thus transfer the input power into the plasma with high efficiency. Typical of the electrothermal technologies are the resistojet and arcjet thrusters, which are using respectively heater and electrical arc discharge in order to heat the propellant. These technologies are having difficulties when dealing with the limitations imposed by the nanosatellite platform. The resistojet is limited by the properties of the heater and chamber materials and nowadays are considered as auxiliary propulsion system for entirely electric propelled satellites.[13] The arcjet thrusters consume energy in the order of several kW.[14,15] There are arcjet thrusters consuming less energy (between 40 and 90 W), but this is still too demanding for the nanosatellite's power budget.[16] The development of microwave electrothermal thruster[17] shows that microwave discharges in cylindrical resonant cavities could be used to heat gas for space propulsion and 100 W–50 kW effective thrusters are constructed.[18,19] Thrusters of the same type also exist using power level <50 W.[20,21]

Nevertheless, there are still several main challenges on the path of electrical propulsion.[22] One such challenge is the insufficiently high service life due to the very strong corrosive action of the plasma. Another challenge is the efficiency of the energy usage and having the capability to adjust the specific impulse as needed. Also, not every electrical propulsion technology is capable of working in both impulse and continuous-wave regimes, which is often desired. Our research team is working on the development of a new type of microwave electrothermal plasma thruster,[23] which is suitable for utilization of onboard nanosatellite platforms following the CubeSat standard. The proposed concept is theorized to have relatively long service life since the contact between the plasma and the thruster's parts is brought to a minimum. The ionization and the subsequent heating process are very fast processes, in the order of microseconds, which allow the thruster to work in both impulse and continuous-wave regimes. By adjusting the power input together with the propellant mass flow rate, all parameters of the thruster can be adjusted and thus affect the thrust levels and the specific impulse. Also, the simple construction is a precedent for low-cost manufacturing, which makes the deorbiting applications of the thruster much more affordable. These features are making the proposed concept worth investigating and developing. The first electrodynamic investigation and optimization of the thruster's dimensions were presented by Ivanov and Kiss'ovski.[23,24] Schematic of the proposed plasma thruster is shown in Figure 1. The radius of the chamber is 1.25 mm, the length is about 10 mm and the diameter of the orifice is 0.2 mm. The dielectric infill of the coaxial transmission line is considered to be PTFE or alumina ceramic. The metal enclosure and the core are made of highly conductive material such as copper.

The propellant gas (argon) is fed through the core metal tube into the gas heating chamber, which is also a resonance chamber for longitudinal plasma resonances[25] and it is denoted as resonant chamber in Figure 1. Microwave power is applied to the resonant chamber through coaxial transmission line. The strong microwave field in the resonator causes breakdown in the gas, production of weakly ionized plasma and excitation of surface waves.[26] The reflection of surface wave from the end of the chamber (metal enclosure) results in a standing wave in the plasma column. The plasma charged particles heat the neutral gas by collisions and the thermal expansion accelerates the gas through the orifice and thus

FIGURE 2 Schematic of the geometry, considered in the computational model

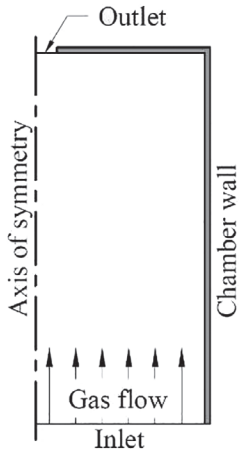

creates thrust. It is important to note that the current investigation considers a simple orifice instead of more sophisticated nozzle profile. The nozzle profile strongly depends on the flow parameters and the used propellant type. The obtained profile of the neutral particles velocity at the orifice can be used as initial conditions for the subsequent nozzle profile design. The gas heating process is vital for the proper performance of the thruster and the current step in this ongoing research is to investigate the plasma processes in the chamber and especially these, which are responsible for heating the neutral particles. Argon is the propellant of choice because it is cheap and relatively safe to work with. Similar thrusters have been investigated with Argon and lighter gasses, such as Helium and Hydrogen[27,28] with the latter gas reaching higher specific impulse. This is due to the fact that the thermal energy gain due to elastic collisions between electrons and heavy particles is higher for lighter gasses, thus the heating is more effective. Heavy gasses such as Xenon and Krypton are more suitable for technologies using electrostatic methods of particle acceleration.

In Section 2 of the paper, particle and energy balance equations are described. The power deposition is assumed with Gaussian shape in radial and longitudinal direction, taking into account the standing wave in the plasma column.[23] The radial steady-state field is calculated by the Poisson equation. The computational model includes electron reactions with the ground state and the first two excited argon levels (−s, −p). The increase of gas temperature in the chamber is obtained by the gas thermal balance equation and the gas flow equation allows calculation of axial velocity through the orifice. The propellant heating processes, the thruster performance parameters and the plasma properties are calculated using the computational model at different propellant mass flow rates and input power level and presented in Section 3.

2 | COMPUTATIONAL MODEL DESCRIPTION

The simplified geometry of the electrothermal thruster considered in the computational model is shown in Figure 2. The argon gas is fed through the inlet contour with specific mass flow rate and fills the chamber. Using Gaussian heat source in the electron energy conservation equation, electrons gain energy and they ionize the neutral gas by direct and step-wise ionization collisions. As a result, the plasma density increases and the heating of the neutral particles due to elastic collisions with the electrons takes place. The heated gas leaves the chamber through the outlet with high velocity and thus creates thrust. The main purpose of the computational model is to estimate the appropriate mass flow rate and input power in order to achieve maximum efficiency and at the same time to stay within the dimensional and power limitations coming with the nanosatellite platforms. It is known that higher plasma density is one way to increase the gas heating, but it also means that more power has to be deposited in order to achieve and sustain that higher plasma density. Therefore, a balance between input power and gas mass flow rate is desired, in order to obtain effective gas heating.

The cylindrical chamber and the equations of the computational model are calculated using COMSOL Multiphysics.

2.1 | Approximations

Several important approximations are adopted within the model: (a) The geometry possesses axial symmetry, which reduces the problem to 2D when we use cylindrical coordinate system, (b) Maxwellian electron energy distribution

function (EEDF), which is justified by the relatively high electron density and thus the strong effect of the Coulomb collisions of electrons, which lead to the Maxwellian shape of EEDF, (c) the momentum transfer frequency does not depend on the applied field frequency $\nu_m(f) = \text{const}$ but it depends on the averaged electron energy (electron temperature, T_e), (d) no electron emission from the walls, (e) radiation losses are not considered, (f) heavy species temperature is equal to the neutral gas temperature.

2.2 | Particle and energy balance equations

The propellant gas chosen is argon, because it is relatively cheap and safe to work with. The model considers the following particles: electrons e^-, argon atoms Ar, argon ions Ar^+, excited atoms Ar(4s) for all 4s excited levels considered as a single lumped level at 11.65 eV and excited atoms Ar(4p) for all 4p excited levels are also considered as a single lumped level at 13.17 eV.

The numerical model is based on a system of partial differential equations. The first one is the particle balance equation[12]:

$$\frac{\partial n_p}{\partial t} + \nabla \cdot \mathbf{G}_p + \mathbf{u}_g \cdot \nabla n_p = S_{c,p}, \tag{1}$$

where index 'p' indicates the particle type except for argon atoms, that is e^-, Ar^+, Ar(4s), Ar(4p). Here n_p indicates species density, $\mathbf{G}_p$ is species flux, $\mathbf{u}_g$ is gas velocity and $S_{c,p}$ is the collision term considering all volume reactions leading to the creation and loss of particles. The particle flux is described within the drift-diffusion approximation by:

$$\mathbf{G}_p = -\nabla(D_p n_p) + \frac{q_p}{|\, q_p \,|}\mu_p n_p \mathbf{E}, \tag{2}$$

where D_p is the diffusion coefficient, q_p is the particle charge, μ_p is the particle mobility and $\mathbf{E}$ is the electrostatic field vector. For neutral particles $q_p = 0$ and the particle flux is determined only by the diffusion. The electron mobility is given by:

$$\mu_e = \frac{|\, q_e \,|}{m_e \nu_m}, \tag{3}$$

where m_e is the electron mass and ν_m is the momentum transfer frequency. The momentum transfer frequency is calculated with $\nu_m = N_{Ar} k_{elastic}(T_e)$, where $k_{elastic}$ is the rate coefficient for elastic collisions listed in Table 1. The electron diffusion coefficient D_e is then obtained using Einstein's relation, that is $D_e = \mu_e T_e$ (eV). The ion mobility is given by[29]:

$$\mu_i = \frac{1.01 \times 10^5}{p_g} \frac{T_g}{273.16} 1.52 \times 10^{-4}, \tag{4}$$

where p_g and T_g are the gas pressure and temperature. Again, the ion diffusion coefficient is expressed using Einstein's relation, that is $D_i = \mu_i T_i$ (eV). The excited particles Ar(4s) and Ar(4p) are assumed to have equal diffusion coefficient given by the expression[30]:

$$D_{Ar(4s)} = D_{Ar(4p)} = \frac{1.16 \times 10^{20}}{N_{Ar}} \left(\frac{T_g}{300} \right)^{0.5}, \tag{5}$$

where N_{Ar} is the density of argon atoms.

The energy balance equation for the electrons is taken in the form[31]

$$\frac{\partial n_e \bar{\varepsilon}_e}{\partial t} + \nabla \cdot \mathbf{G}_{\varepsilon,e} + \mathbf{u}_g \cdot \nabla n_e \bar{\varepsilon}_e = q\mathbf{E} \cdot \mathbf{G}_e + n_e \Delta \bar{\varepsilon}_e + (Q_{bg} + Q_{Gauss})/q_e, \tag{6}$$

where $\bar{\varepsilon}_e$ indicates the averaged energy over the energy distribution function, $\mathbf{G}_{\varepsilon,e}$ is the electron energy flux and $\Delta\bar{\varepsilon}_e$ is the electron energy transfer due to collisions. The term Q_{bg} represents weak background power density maintaining

TABLE 1 Reactions considered in the computational model

No.	Reaction	Rate coefficient (m^3/s)	Description	Ref.
1.	$Ar + e^- \rightarrow Ar(4s) + e^-$	$k_1 = 4.5486 \times 10^{-17} T_e^{0.5} \exp[(E_{Ar} - E_{Ar(4s)}) q_e/(k_b T_e)]$	Excitation	[32]
2.	$Ar + e^- \rightarrow Ar(4p) + e^-$	$k_2 = 1.8207 \times 10^{-17} T_e^{0.71} \exp[(E_{Ar} - E_{Ar(4p)}) q_e/(k_b T_e)]$	Excitation	[33]
3.	$Ar(4s) + e^- \rightarrow Ar(4p) + e^-$	$k_3 = 7.5235 \times 10^{-15} T_e^{0.51} \exp[(E_{Ar(4s)} - E_{Ar(4p)}) q_e/(k_b T_e)]$	Excitation	[33]
4.	$Ar(4s) + e^- \rightarrow Ar + e^-$	$k_4 = 4.4557 \times 10^{-18} T_e^{0.5}$	Superelastic collision	[32]
5.	$Ar(4p) + e^- \rightarrow Ar + e^-$	$k_5 = 5.0719 \times 10^{-19} T_e^{0.71}$	Superelastic collision	[33]
6.	$Ar(4p) + e^- \rightarrow Ar(4s) + e^-$	$k_6 = 2.5360 \times 10^{-15} T_e^{0.51}$	Superelastic collision	[33]
7.	$Ar + e^- \rightarrow Ar^+ + 2e^-$	$k_7 = 1.1789 \times 10^{-16} T_e^{0.5} \exp[(E_{Ar} - E_{Ar^+}) q_e/(k_b T_e)]$	Ionization	[32]
8.	$Ar(4s) + e^- \rightarrow Ar^+ + 2e^-$	$k_8 = 1.2859 \times 10^{-17} T_e^{0.67} \exp[(E_{Ar(4s)} - E_{Ar^+}) q_e/(k_b T_e)]$	Ionization	[33]
9.	$Ar(4p) + e^- \rightarrow Ar^+ + 2e^-$	$k_9 = 5.9682 \times 10^{-16} T_e^{0.61} \exp[(E_{Ar(4p)} - E_{Ar^+}) q_e/(k_b T_e)]$	Ionization	[33]
10.	$Ar + e^- \rightarrow Ar + e^-$	$k_{elastic}(T_e)$ relation obtained by integrating the scattering cross sections over the EEDF using BOLSIG+	Elastic collision	[34]

Note: All units are in SI unless otherwise noted.

electron densities $n_e \leq 1 \times 10^{13}\ m^{-3}$ for the considered discharge period. This approach ensures more stable numerical calculations and at the same time has negligible effect on the final results. Q_{Gauss} is a power deposition term having the following Gaussian shape:

$$Q_{Gauss}(r,z) = A_{Gauss} \exp\left(-\frac{(z-z_0)^2}{2\sigma_z^2} + \frac{r^2}{2\sigma_r^2}\right)\ W/m^3, \tag{7}$$

where A_{Gauss} is the power density amplitude, r and z are cylindrical coordinates, z_0 is half of the chamber length and ensures that the maximum of the z-component is in the middle of the heating chamber, σ_z and σ_r define the width in, respectively, the z-direction and the r-direction. Figure 3 depicts the two-dimensional Gaussian profile used in the computational model. This term approximates the heating effect of the microwave field on the plasma electrons with an effective spatial profile. The exact shape of the power density profile of the electron heating due to the MW field is not critical as the current model investigates the ability of the plasma to heat the neutral gas and not the actual plasma creation and sustenance. Moreover, the significant electron thermal conductivity leads to weaker sensitivity of the obtained results from the exact shape of the plasma heating distributions.

The electron energy flux[31] is:

$$\mathbf{G}_{\varepsilon,e} = -D_{\varepsilon,e} \nabla(n_e \bar{\varepsilon}_e) - \frac{q_e}{|q_e|} \mu_{\varepsilon,e} \mathbf{E} n_e \bar{\varepsilon}_e, \tag{8}$$

where $\mu_{\varepsilon,e} = (5/3)\mu_e$ is electron energy mobility and $D_{\varepsilon,e} = \mu_{\varepsilon,e} T_e$ (eV) is the electron energy diffusion coefficient.

2.3 | Internal electrostatic field

The internal electric field induced by the plasma charges is calculated using the Poisson equation:

$$\nabla^2 \phi = -\rho_q/\varepsilon_0, \tag{9}$$

where ϕ is the electric potential, ρ_q is the charge density and ε_0 is the vacuum dielectric permittivity.

2.4 | Considered reactions

All considered reactions in the computational model are listed in Table 1.

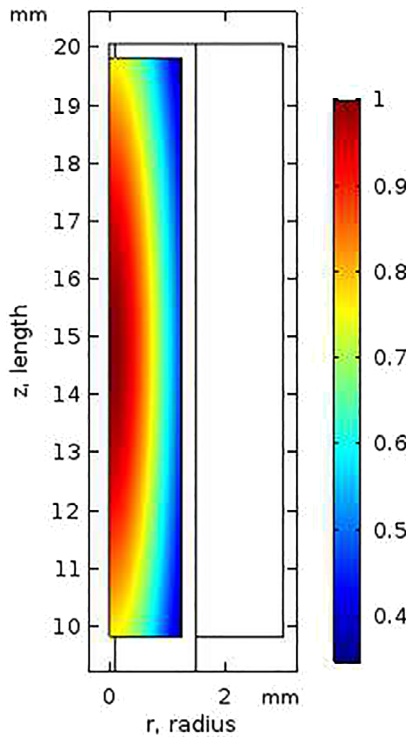

FIGURE 3 Gaussian heat source profile included in the electron energy balance equation

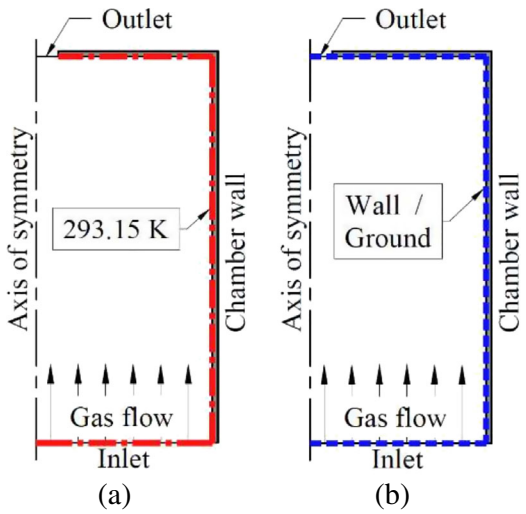

FIGURE 4 (a) Boundary condition for gas thermal balance. (b) Boundary condition for plasma particles

2.5 | Gas flow equations

The most meaningful result of the current study is the gas velocity profile at the outlet. This gas velocity profile could be used as initial condition for the further design of sophisticated nozzle profile as a next step in the current ongoing research. For this purpose, the flow is considered as turbulent flow and is described using Navier–Stokes equation as follows:

$$\rho_{\mathrm{g}}\frac{\partial \mathbf{u}_{\mathrm{g}}}{\partial t} + \rho_{\mathrm{g}}(\mathbf{u}_{\mathrm{g}}\cdot\nabla))\mathbf{u}_{\mathrm{g}} = \nabla\cdot[-p_{\mathrm{g}}\mathbf{I} + (\mu_{\mathrm{g}} + \mu_{\mathrm{g,T}})(\nabla\mathbf{u}_{\mathrm{g}} + (\nabla\mathbf{u}_{\mathrm{g}})^{\mathrm{T}})], \tag{10}$$

$$\rho_g\nabla\cdot\mathbf{u}_g = 0, \tag{11}$$

where ρ_{g} is the gas density, p_{g} is the gas pressure, $\mathbf{I}$ is the unit matrix, μ_{g} is the gas viscosity, $\mu_{\mathrm{g,T}}$ is the turbulent gas viscosity and superscript 'T' stands for the tensor transpose operation.

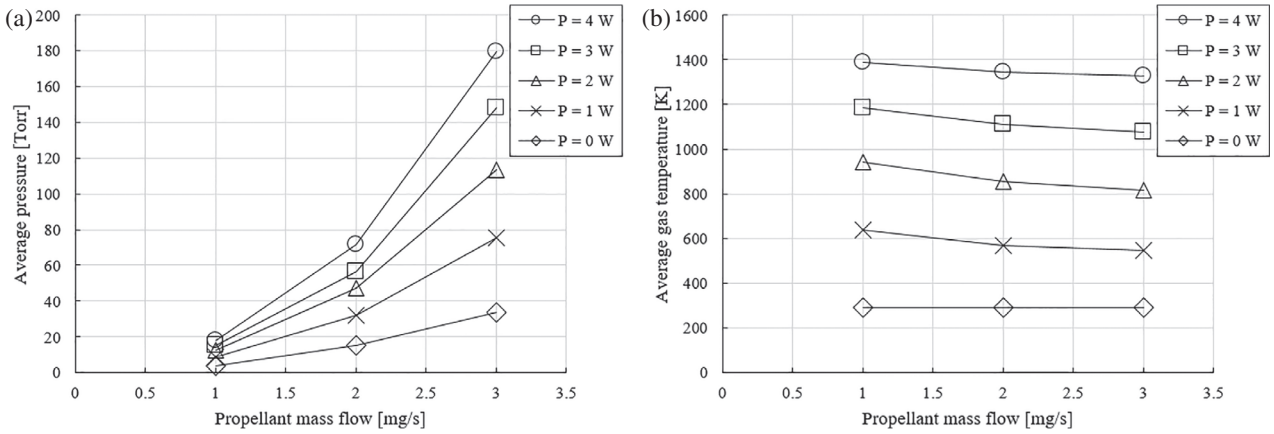

FIGURE 5 (a) Average pressure in the plasma chamber at different mass flow rates and input power, P. (b) Average gas temperature in the plasma chamber at different mass flow rates and input power, P

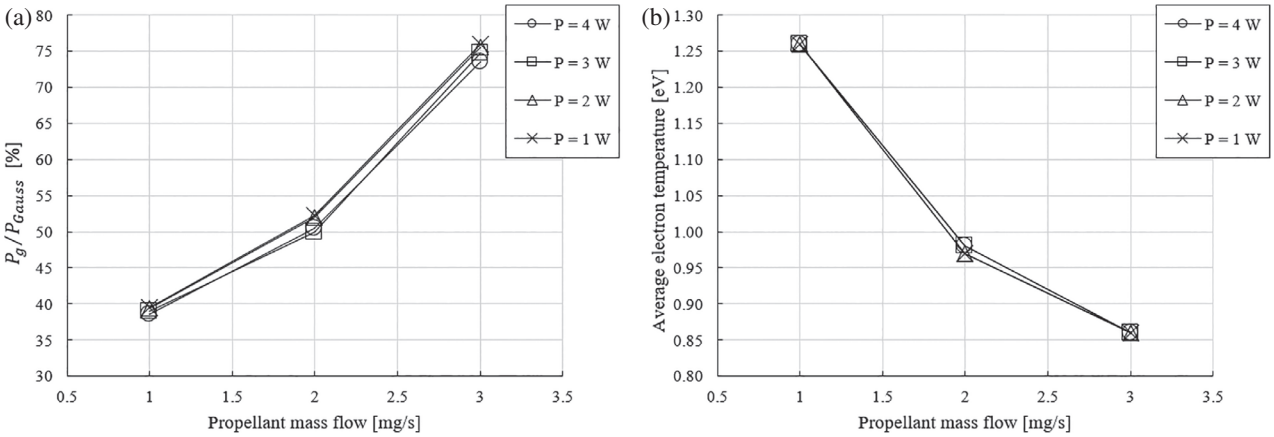

FIGURE 6 (a) Gas heating power to input power percentage ratio. (b) Average electron temperature change at different mass flow rates and input power levels

For better accuracy, a $k-\varepsilon$ turbulent model is used.[35] This model utilizes two additional dependent variables: the turbulent kinetic energy k, and the turbulent dissipation rate ε. The turbulent viscosity is modelled as

$$\mu_{\mathrm{g,T}} = \rho_{\mathrm{g}} C_{\mu} \frac{k^2}{\varepsilon}, \tag{12}$$

where $C_{\mu} = 0.09$ is a model constant. The transport equation for k is

$$\rho_{\mathrm{g}} \frac{\partial k}{\partial t} + \rho_{\mathrm{g}} \mathbf{u}_{\mathrm{g}} \cdot \nabla k = \nabla \cdot \left(\left(\mu_{\mathrm{g}} + \frac{\mu_{\mathrm{g,T}}}{\sigma_k} \right) \nabla k \right) + P_k - \rho_{\mathrm{g}} \varepsilon, \tag{13}$$

where $\sigma_k = 1.0$ is model constant and the production term P_k is

$$P_k = \mu_{\mathrm{g,T}} \left(\nabla \mathbf{u}_{\mathrm{g}} : (\nabla \mathbf{u}_{\mathrm{g}} + (\nabla \mathbf{u}_{\mathrm{g}})^{\mathrm{T}}) - \frac{2}{3} (\nabla \cdot \mathbf{u}_{\mathrm{g}})^2 \right) - \frac{2}{3} \rho_{\mathrm{g}} k \nabla \cdot \mathbf{u}_{\mathrm{g}}. \tag{14}$$

The transport equation for ε is

$$\rho_{\mathrm{g}} \frac{\partial \varepsilon}{\partial t} + \rho_{\mathrm{g}} \mathbf{u}_{\mathrm{g}} \cdot \nabla \varepsilon = \nabla \cdot \left(\left(\mu_{\mathrm{g}} + \frac{\mu_{\mathrm{g,T}}}{\sigma_{\varepsilon}} \right) \nabla \varepsilon \right) + C_{\varepsilon_1} \frac{\varepsilon}{k} P_k - C_{\varepsilon_2} \rho \frac{\varepsilon^2}{k}. \tag{15}$$

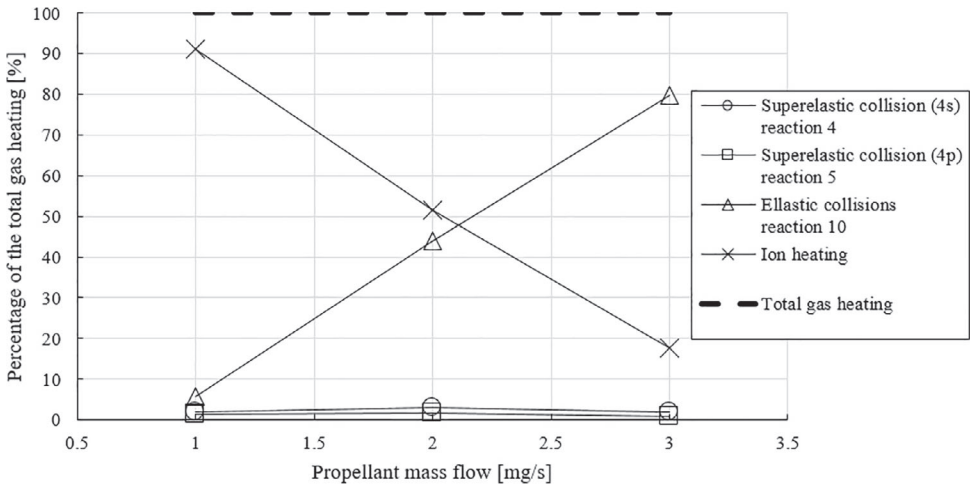

FIGURE 7 Comparison of gas heating terms contribution from Equation (17) at different mass flow rates

where $\sigma_\varepsilon = 1.3$, $C_{\varepsilon_1} = 1.44$ and $C_{\varepsilon_2} = 1.92$ are model constants. All model constants are determined from experimental date.[35]

2.6 | Gas thermal balance equation

The gas heating is an important process in the current study because it determines the gas flow velocity through the chamber outlet. For its description, a gas thermal balance equation is used as follows:

$$\rho_g C_p \frac{\partial T_g}{\partial t} + \rho_g C_p \mathbf{u}_g \cdot \nabla T_g - \nabla \cdot (k_g \nabla T_g) = Q_g, \tag{16}$$

where C_p is the specific heat of argon, k_g is the argon conductivity and Q_g is the heat source, which in our case is entirely coming from the plasma processes. The heat source term includes all processes, which result in energy lost by the electrons and transferred to the neutral particles as well as the energy transferred from the ions to the gas mainly by charge-exchange collisions. The ions are gaining energy from the internal electrostatic field. The total gas heat source is:

$$Q_g = k_4 n_e n_{Ar(4s)} q_e 11.65(\text{eV}) + k_5 n_e n_{Ar(4p)} q_e 13.17(\text{eV}) + \frac{3 m_e m_{Ar}}{(m_e + m_{Ar})^2} n_e n_{Ar} k_{elastic} q_e (T_e(\text{eV}) - T_g(\text{eV})) + \mathbf{j}_{ion} \cdot \mathbf{E}, \tag{17}$$

where m_{Ar} is the mass of an argon atom. The first and second terms represent the heating due to inelastic collisions. The third term accounts for the elastic collisions and the last term is the ion heating as scalar product of the ion current $\mathbf{j}_{ion}$ and the internal electrostatic field $\mathbf{E}$.

2.7 | Boundary conditions

The model is non-quasi-neutral and the particle fluxes to the walls need to be imposed as boundary conditions. Assuming non-emitting walls (without secondary electron emission), the boundary condition for the electron particle balance at the walls is:

$$\mathbf{n} \cdot G_e = \frac{1}{2} v_{th,e} n_e, \tag{18}$$

where $\mathbf{n}$ is the normal vector to the wall and $v_{th,e} = \sqrt{8 k_b T_e / \pi m_e}$ is the electron thermal velocity. The boundary condition for electrons energy balance is given by:

$$\mathbf{n} \cdot G_{\varepsilon,e} = \frac{5}{6} v_{th,e} n_e \bar{\varepsilon}_e, \tag{19}$$

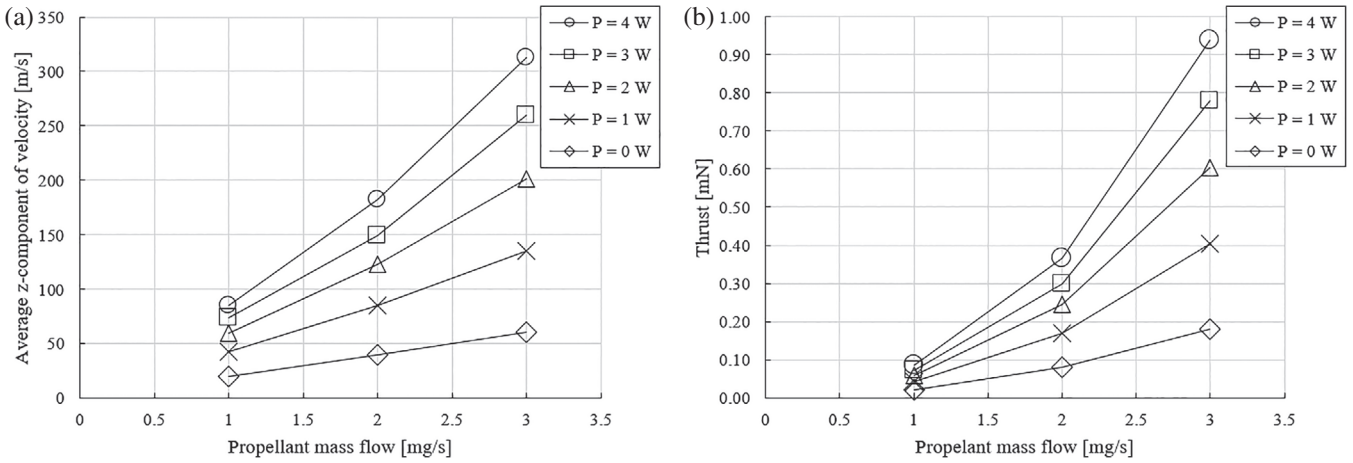

FIGURE 8 (a) Average z-component of neutral particles velocity at the outlet at different power input levels and mass flow rates. (b) Generated thrusts at different mass flow rates and input power

For the heavy species, the boundary condition is:

$$\mathbf{n} \cdot \mathbf{G}_{\mathrm{h}} = \frac{1}{4} v_{\mathrm{th,h}} n_{\mathrm{h}} + \max\left(\frac{q_{\mathrm{h}}}{|\, q_{\mathrm{h}} \,|} \mu_{\mathrm{h}} n_{\mathrm{h}} \mathbf{E} \cdot \mathbf{n}, 0 \right), \tag{20}$$

where index 'h' indicates the heavy particle type. For the excited Ar(4s) and Ar(4p) atoms $q_{\mathrm{h}} = 0$. The thermal velocity for the heavy species is taken as $v_{\mathrm{th,h}} = \sqrt{8 k_{\mathrm{b}} T_{\mathrm{g}} / \pi m_{\mathrm{h}}}$.

The boundary conditions for the gas thermal balance are shown in Figure 4a. It is considered that the chamber walls and the inlet are sustained at constant temperature 293.15 K. This is somewhat reasonable assumption, because it is expected that the thermal management subsystem of the nanosatellite will maintain temperatures suitable for nominal performance of the onboard batteries. The boundary condition for the plasma particles is shown in Figure 4b. At first glance, putting the outlet as a "Wall" looks a bit odd, but the expected ionization degree is $\alpha < 0.001$ and therefore the number of expelled ions and excited atoms is negligible in comparison with the number of neutral particles, hence this approach does not influence the results too much. The sticking coefficient is taken as 1 for all particles at the walls. The interactions of the particles with the walls are given by the conversions $P \rightarrow \mathrm{Ar}$, where $P = \mathrm{Ar(4s)}$, $\mathrm{Ar(4p)}$ and Ar^+.

With respect to the boundary condition for the Poisson equation, the same contours, shown in Figure 4b, are defined as "Ground", which ensures more stable solution and is considered enough for this initial stage of the model.

3 | RESULTS AND DISCUSSION

In the current study, the effect of propellant mass flow rate and power input on the propellant heating efficiency is investigated. For better understanding of the results and easier comparison with similar thrusters, the corresponding thruster performance is shown both with heating and without heating (cold flow) of the propellant. Figure 5a,b depicts respectively the established average pressure and the average gas temperature in the plasma chamber.

It can be observed that though the pressure increases significantly with the mass flow rate, the gas temperature drops slightly due to the increased convective cooling by the gas. In fact, the combination of low neutral particle density with high gas temperature does not guarantee effective performance of the thruster. For this purpose, the input and output energy balance of the system is further investigated. Figure 6a shows the ratio of gas heating power relative to the input power.

It is easily observable that the ratio stays almost the same at different input power levels, but greatly increases at higher mass flow rates. This is related to the significant increase of the gas pressure in the chamber and thus to the more significant contribution of the collisional energy transfer from the electrons to the gas mainly due to elastic collisions. For more effective heating of the neutral gas from the plasma processes, higher ratio is of course desired. On the other hand, greater mass flow rates and thus pressure lead to drop in the average electron temperature, as shown in Figure 6b and

calculated using

$$T_{\mathrm{e,avg}} = \frac{2}{3}\frac{\int_V n_\mathrm{e}\bar{\varepsilon}_\mathrm{e}\,dV}{\int_V n_\mathrm{e}\,dV}. \tag{21}$$

This behaviour is natural since the increased pressure leads to more efficient (frequent) ionization and thus lower electron temperature is required to sustain the plasma. Figure 7 depicts how the contribution of each term from the gas heating Equation (17) is changing with the mass flow rate at fixed input power of 2 W.

It can be seen that the elastic collisions contribution to the gas heating greatly increases at higher mass flow rates and higher pressure respectively. The figure shows a significant change in the energy transfer mechanism to the neutral gas. At low gas flow and pressure, the mean free path of the electrons does not allow for significant energy transfer to the neutrals but instead they transfer energy to the ions through the electric field and then the ions transfer the energy to the neutral gas mainly due to the charge-transfer mechanism, included implicitly in the ion mobility. At higher pressure, the electron elastic collisions become the dominant mechanism while the ion losses diminish.

Figure 8a depicts the relation of the different propellant mass flow rates and input power to the average z-component of the velocity of the neutral particles at the outlet. It can be observed that higher input power at lower mass flow rates leads to smaller increase in the exhaust velocity of the propellant in comparison to higher mass flow rates. This is the result of the more effective gas heating at higher mass flow rates discussed above. It is important to note that the properties of the propellant flow at the outlet can be used as input values for the design of de Laval nozzle, which could further increase the neutral particles velocity and thus increase the specific impulse of the thruster. Figure 8b shows the thrust that each of the mass flow rate and input power combinations generate. It can be seen that the generated thrust can reach levels in the order of 1 mN, which could potentially provide adequate propulsion assistance of CubeSats with mass up to 4 kg.

4 | CONCLUSIONS

The main aim of this study is to investigate the efficiency of the heating using the charged particles in the plasma column as a heating source. The proposed thruster is suitable for the needs of the CubeSat satellite platforms and comes in line with the imposed power, mass and size limitations. For this purpose, a numerical investigation has been conducted by combining gas discharge model with turbulent flow model, utilizing a set of particle balance equations, Poisson, Navier–Stokes, electron and gas thermal balance equations. The heating of the propellant is then investigated using different propellant mass flow rates and power input levels. The electrons are heated using Gaussian profile heat source. The neutral gas is then heated by superelastic and elastic collisions as well as ion heating. The results show that the desired combination of power input level and propellant mass flow rate exists in order to provide an effective and adequate propulsion subsystem for CubeSat missions. It was found that relatively significant gas flow is needed in order to increase the pressure in the chamber, which provides more efficient energy transfer from the charged species to the neutral gas. The current research serves as a basis in the ongoing development of the proposed microwave electrothermal thruster.

ACKNOWLEDGMENTS

This research is supported by the Bulgarian Ministry of Education Science Fund (Contract No. KP-06-OPR 01/1), and the National Research Programme "Young scientists and postdoctoral students" approved by DCM No. 577/August 17, 2018.

DATA AVAILABILITY STATEMENT

Research data are not shared.

REFERENCES

[1] J. Bradford, C. Williams, S. DelPozzo, Nano/microsatellite Market Forecast, 10th ed. **2020** https://www.spaceworks.aero/nano-microsatellite-forecast-10th-edition-2020/ (accessed: March 2021).
[2] I. Levchenko, M. Keidar, J. Cantrell, Y. Wu, H. Kuninaka, K. Bazaka, S. Xu, *Nature* **2018**, *562*, 185.
[3] I. Levchenko, S. Xu, Y. L. Wu, K. Bazaka, *Nat Astron* **2020**, *4*, 1012.
[4] D. Greenbaum, *Science* **2020**, *20*, 922.
[5] S. Mazouffre, *Plasma Sources Sci. Technol.* **2016**, *25*, 27.
[6] I. Levchenko, K. Bazaka, Y. Ding, Y. Raitses, S. Mazouffre, T. Henning, P. J. Klar, S. Shinohara, J. Schein, L. Garrigues, M. Kim, *Appl. Phys. Rev.* **2018**, *5*, 011104.

[7] Y. Takao, K. Eriguchi, K. Ono, *J. Appl. Phys.* **2007**, *101*, 123307.
[8] J. Lucas, G. Teel, J. Kolbeck, M. Keidar, *AIP Adv.* **2016**, *6*, 025311.
[9] C. Charles, R. Boswell, *Plasma Sources Sci. Tech.* **2012**, *21*, 022002.
[10] S. Bilén, C. Valentino, M. Micci, D. Clemens, *Proc. 41st Joint Propulsion Conf.* **2005** (AIAA-2005-3699), 9.
[11] Z. Kiss'ovski, M. Kolev, A. Ivanov, S. Lishev, I. Koleva, *J. of Phys. D: Appl. Phys* **2009**, *42*, 182004.
[12] S. Kolev, A. Bogaerts, *Plasma Sources Sci. Tech.* **2014**, *24*, 015025.
[13] G. Cifali, S. Gregucci, E. Andreussi, M. Andrenucci, *Proc. 35th IEPC* **2017** (paper IEPC-2017-371), pp 1–9.
[14] R. Welle, *Proc. of The 35th ASME* **1997** (AIAA paper 97–0794).
[15] M. Auweter-Kurtz, A. Sasoh, *J. Propul. Power* **1998**, *14*, 11.
[16] H. Horisawa, I. Kimura, *Vacuum* **2000**, *59*(106), 12.
[17] P. Balaam, M. Micci, *25th AIAA/ASME/SAE/ASEE JPC* **1989** (AIAA paper 89–2380).
[18] J. Brandenburg, J. Kline, D. Sullivan, *IEEE Trans. Plasma Sci.* **2005**, *33*, 776.
[19] M. S. Yildiz, U. Kokal, M. Celik, *53rd AIAA/SAE/ASEE Joint Propulsion Conf* **2017** (AIAA-2017-4725).
[20] Y. Takao, T. Takahashi, K. Eriguchi, K. Ono, *Pure Appl. Chem.* **2008**, *80*, 2013.
[21] S. E. Gallucci, M. Micci, S. G. Bilén, *Proc. 35th IEPC* **2017** (IEPC-2017-296).
[22] I. Levchenko, S. Xu, S. Mazouffre, D. Lev, D. Pedrini, D. Goebel, L. Carrigues, F. Taccogna, K. Bazaka, *Phys. Plasmas* **2020**, *27*, 020601.
[23] S. Ivanov, Zh. Kiss'ovski, *Proc. 7th RGCEP* **2018**.
[24] S. Ivanov, Zh. Kiss'ovski, *Proc. 36th IEPC* **2019** (IEPC-2019-647).
[25] S. Nonaka, *J. Phys. Soc. Jpn.* **1990**, *59*, 1623.
[26] H. Schlüter, A. Shivarova, *Phys. Reports* **2007**, *443*, 121.
[27] T. Takahashi, Y. Takao, Y. Ichida, K. Eriguchi, K. Ono, *Phys. Plasmas* **2011**, *18*, 063505.
[28] M. S. Yildiz, M. Celik, *IEEE Trans. Plasma Sci.* **2017**, *45*, 2314.
[29] E. McDaniel, E. Mason, Mobility and Diffusion of Ions in Gases, Springer, Hoboken NJ **1973**.
[30] C. Ferreira, J. Loureiro, A. Ricard, *J. Appl. Phys.* **1985**, *57*, 9.
[31] G. Hagelaar, L. Pitchford, *Plasma Sources Sci Technol.* **2005**, *14*, 12.
[32] Y. Kabouzi, D. Graves, E. Castaños-Martínez, M. Moisan, *Phys. Rev. E* **2007**, *75*, 14.
[33] S. Ashida, C. Lee, M. Lieberman, *J. Vac. Sci. Technol. A* **1995**, *13*, 10.
[34] L. L. Alves, *J. Phys. Conf. Series* **2014**, *565*(1), 012007.
[35] D. Wilcox, Turbulence Modeling for CFD, 2nd ed., DCW Industries, La Canada, California, **1998**.

How to cite this article: Ivanov S, Kolev S, Kiss'ovski Z. Numerical investigation of the plasma processes for propellant heating in electrothermal plasma thruster for nanosatellites. *Contributions to Plasma Physics*. 2021;e202100017. https://doi.org/10.1002/ctpp.202100017